

---

# FUSION OF COMPLEX NETWORKS AND RANDOMIZED NEURAL NETWORKS FOR TEXTURE ANALYSIS

---

Lucas C. Ribas<sup>1</sup>, Jarbas Joaci de Mesquita Sá Junior<sup>3</sup>, Leonardo F. S. Scabini<sup>2</sup>, and Odemir M. Bruno<sup>1,2</sup>

<sup>1</sup>São Carlos Institute of Physics, University of São Paulo (USP), PO Box 369, 13560-970, São Carlos, SP, Brazil.  
Scientific Computing Group

<sup>2</sup>Institute of Mathematics and Computer Science, University of São Paulo (USP), USP, Avenida Trabalhador são-carlense, 400, 13566-590, São Carlos, SP, Brazil.

<sup>3</sup>Curso de Engenharia da Computação, Programa de Pós-Grad. em Eng. Elétrica e de Computação, Campus de Sobral, Universidade Federal do Ceará, Rua Coronel Estanislau Frota, 563, Centro, Sobral, Ceará, CEP: 62010-560, Brasil

## ABSTRACT

This paper presents a high discriminative texture analysis method based on the fusion of complex networks and randomized neural networks. In this approach, the input image is modeled as a complex networks and its topological properties as well as the image pixels are used to train randomized neural networks in order to create a signature that represents the deep characteristics of the texture. The results obtained surpassed the accuracy of many methods available in the literature. This performance demonstrates that our proposed approach opens a promising source of research, which consists of exploring the synergy of neural networks and complex networks in the texture analysis field.

## 1 Introduction

Most of computer vision applications consider texture as a key factor to image discrimination, thus texture analysis has been a constant research field since the 1960s. The texture is a visual pattern related to the object surface, which in an image is represented by the pixel spatial organization. However, the interpretation of texture is ambiguous, thus there is no formal definition to the term that is widely accepted by the scientific community. This resulted in an extensive and heterogeneous literature of texture analysis methods proposed along the years [8, 39, 65]. Usually, texture descriptors are applied in different areas such as industrial inspection [41], geology [62], medicine [14], material science [68], and so on.

Classical texture analysis techniques can be grouped into four different approaches: statistical, spectral, structural, model-based methods [66]. The earlier and most diffused methods are statistical-based, such as variants of gray-level co-occurrence matrices (GLCM) [31, 49] and local binary patterns (LBP) [10, 45]. Spectral methods explore texture in the frequency domain, some examples are Gabor filters [34] and wavelet transform [21]. On the other hand, structural methods consider texture as a combination of smaller elements, called textons, that compose the overall texture as a spatially organized pattern. A common approach of this kind of analysis is the Morphological decomposition [37]. Finally, model-based methods represent textures through sophisticated mathematical models and estimating its parameters. Common methods of this category include Fractal models [2–4, 12, 23, 56] and stochastic models [50]

Besides classical methods, more recent and innovative techniques are addressing texture differently, achieving promising results. An example is the set of techniques that use learning, such as descriptors based on a vocabulary of scale invariant feature transform (SIFT) [17], often called bag-of-visual-words (BOVW). Methods based on image complexity analysis are also gaining attention such as cellular automata [19] and complex networks (CN) [4, 26, 57, 58, 64]. In particular, methods based on the CN theory have achieved promising results due to its capacity to represent the relation among structural elements of texture. However, the problem of how to achieve more satisfactory modeling (i.e., a lesser number of parameters) and new ways of characterizing the network remains a challenge to overcome.

In this paper, we propose a novel approach that combines complex networks and randomized neural networks (RNN) in order to obtain a texture signature. Complex networks is attracting increasing attention due to its flexibility and generality for representing many real-world systems, including texture images. On the other hand, a randomized neural

network is a neural network with a unique hidden layer and a very fast learning algorithm, which has been used in many pattern recognition tasks. Here we first model the texture image as a directed network, representing the information about the pixels and its neighbors as vertices and edges. To characterize the texture, the topological properties from the modeled network and the image pixels are used to train a randomized neural network, and the set of output weights is used as a feature vector that represents discriminative characteristics of the texture. Experimental results on four databases demonstrated a better performance of the proposed method when compared to other methods of the literature.

The remainder of this paper is organized as follows. Section 2 describes the fundamentals of complex networks and randomized neural networks. A novel method for texture classification based on fusion of complex networks and randomized neural networks is presented in Section 3. Section 4 describes the databases and experiments performed to evaluate the proposed method. The discussion about the results achieved and comparisons are presented in Section 5. Finally, in Section 6, we conclude the work with some remarks.

## 2 Background

### 2.1 Complex networks

Almost any natural phenomena can be modeled as networks by defining a set of entities and establishing a criterion of relation between them. Some classical examples are the internet, composed of various connected computers and routers, and a network of a cell, describing chemicals connected by chemical reactions. Complex networks are part of an area known as network science [6]. Network science is strongly based on graph theory. In the last decades, works have shown patterns present in many networks or graphs, which were then understood as a structural characteristic of some models such as the scale-free [7] and the small-world [61]. These findings have caused increasing interest from the scientific community on the study of complex networks, creating a new multidisciplinary research field.

The theoretical foundations of this area arise from of the intersection of the graph theory, physics, mathematics, statistics and computer science. Therefore, CN has been employed as a powerful tool for pattern recognition [43], where natural systems of many areas are modeled as networks and then quantified through its topological structure. CN applications are found in various areas of science, such as, physics, social sciences, biology, mathematics, ecology, medicine, computer science, linguistic, neuroscience, among others [18].

Formally, a network or graph  $G$  is described by a tuple of vertices and edges  $(V, E)$ . Let  $v_i$  be a vertex of the set  $V = \{v_1, \dots, v_n\}$ . An edge  $e_{v_i, v_j}$  represents a connection between two vertices  $v_i$  and  $v_j$ , so the set  $E = \{e_{v_i, v_j}, \dots\}$  is composed of all edges connecting vertices of  $V$ . The network can also be directed, in this case, the edges  $e_{v_i, v_j}$  have a direction from  $v_i$  to  $v_j$ . In most of the CN applications, the first step is to define how to model the target problem as a network, thus defining what are the vertices and what are the edges. Once  $G$  is properly built, many measures can be computed to quantify its structure, varying from centrality, path-based measures, community structure, and many more [15]. Moreover, the structure of a real network is the result of the continuous evolution of the forces that formed it, and certainly affects the function of the system [9]. Therefore, the network dynamics can be analyzed by the characterization of its structural evolution in function of time or some modeling parameter.

### 2.2 Randomized neural networks

Randomized neural networks [32, 51, 52, 59] are neural networks composed of two neuron layers (hidden and output layer), each one with a different role in the regression/classification task. The hidden layer has its neural weights determined randomly according to a probability distribution (for instance, a uniform or normal distribution). Its purpose is to project non-linearly the input data in another dimensional space where it is more likely that the feature vectors are linearly separable, as stated in Cover's theorem [16]. In turn, the output layer aims to linearly separate these projected feature vectors using the least-squares method.

Mathematically, letting  $X = [\vec{x}_1, \vec{x}_2, \dots, \vec{x}_N]$  be a matrix of input feature vectors (including +1 for bias weight) and  $D = [\vec{d}_1, \vec{d}_2, \dots, \vec{d}_N]$  be the corresponding labels, the first step is to build the matrix of hidden neuron weights  $W$  of dimensions  $Q \times (p + 1)$ , where  $Q$  and  $p$  are the number of hidden neurons and the number of attributes in each input feature vector, respectively.

Next, the output of the hidden layer for all the feature vectors  $\vec{x}_i$  ( $i \in 1, \dots, N$ ) can be obtained by  $Z = \phi(WX)$ , where  $\phi(\cdot)$  is generally a sigmoid or hyperbolic tangent function. Thus, this matrix of projected vectors  $Z = [\vec{z}_1, \vec{z}_2, \dots, \vec{z}_N]$  (including +1 for bias weight) can be used to compute the output neuron weights, according to the following equation

$$M = DZ^T(ZZ^T)^{-1}, \quad (1)$$

where  $Z^T(ZZ^T)^{-1}$  is the Moore-Penrose pseudo-inverse [44, 54].

Sometimes, the matrix  $ZZ^T$  becomes singular (that is, without inverse), or close to singular, which results in unstable results in Equation 1. In order to avoid these drawbacks, it is possible to use the Tikhonov regularization [13, 60], according to

$$M = DZ^T(ZZ^T + \lambda I)^{-1}, \quad (2)$$

where  $0 < \lambda < 1$  and  $I$  is the identity matrix.

### 3 Proposed method

In this section, we describe the proposed method that combines a new texture modeling in complex networks and randomized neural networks for texture characterization.

#### 3.1 Modeling texture as directed CN

Let  $I$  be an image composed of pixels  $i$ , which have as Cartesian coordinates  $x_i$  and  $y_i$ . In gray-scale images, each pixel has an intensity represented by an integer value  $I(i) \in [0, L]$ , where  $L$  is the highest gray-level value. To model a texture image as a directed network, each pixel  $i$  is mapped as a vertex  $v_i \in V$  of a network  $R$ . The set of edges  $E$  is built connecting two vertices  $v_i$  and  $v_j$ , which represent two pixels  $i$  and  $j$ , by a directed edge from  $v_i$  to  $v_j$ ,  $e_{v_i, v_j} \in E$ , if the Euclidean distance between them is less than or equal to a radius  $r$  and  $I(i) \leq I(j)$ , according to

$$E = \{e_{v_i, v_j} \in E \mid \text{dist}(v_i, v_j) \leq r \wedge I(i) < I(j)\}, \quad (3)$$

where  $\text{dist}(v_i, v_j) = \sqrt{(x_i - x_j)^2 + (y_i - y_j)^2}$  is the Euclidean distance between two pixels. Each edge has a weight  $w(e_{v_i, v_j})$  defined as

$$w(e_{v_i, v_j}) = \begin{cases} \frac{|I(i) - I(j)|}{L}, & \text{If } r = 1 \\ \frac{\left(\frac{\text{dist}(v_i, v_j) - 1}{r - 1}\right) + \left(\frac{|I(i) - I(j)|}{L}\right)}{2}, & \text{Otherwise.} \end{cases} \quad (4)$$

It is worth mentioning that the direction of the edges is determined by the pixel gray-levels. In other words, an edge points to the vertex that represents a pixel with greater intensity. If both intensities are equal, the edge is bidirectional. It is also important to stress that the value  $r$  is the unique parameter of modeling and determines the size of the neighborhood of each vertex. Thus, as  $r$  increases, the reach of connection and the degree of vertices increase as well. This procedure makes the analysis of the behavior of this evolution an interesting way of studying these networks. Figure 1 shows the modeling of a texture image as a directed network for different values of  $r$ .

#### 3.2 Proposed signature based on RNN

Our method aims to use as texture signature the weights of the output layer of the RNN trained with information from the modeled complex networks. For this, three sources of information are considered for each vertex: out-degree, weighted out-degree, and weighted in-degree. As the out-degree is directly related to the in-degree in the modeled networks (i.e. the sum of these two degrees is equal in all the vertices) and, therefore, provide the same information, we considered only the out-degree.

The out-degree  $k_{v_i}$  of a vertex  $v_i$  represents the number of out-edges connected to other vertices,

$$k_{v_i} = \sum_{v_j \in V} \begin{cases} 1, & e_{v_i, v_j} \in E \\ 0, & \text{otherwise.} \end{cases} \quad (5)$$

On the other hand, the weighted out-degree  $ks_{v_i}$  is given by the sum of the weights of the out-degree edges of a vertex  $v_i$ ,

$$ks_{v_i} = \sum_{v_j \in V} \begin{cases} w(e_{v_i, v_j}), & e_{v_i, v_j} \in E \\ 0, & \text{otherwise.} \end{cases} \quad (6)$$

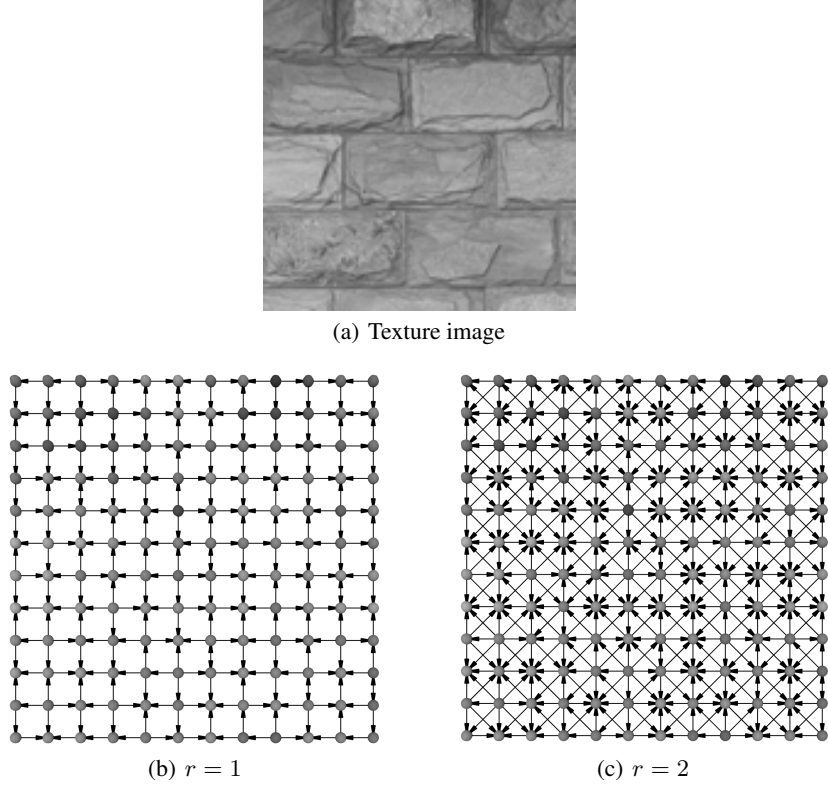


Figure 1: Examples of a texture image modeled as a directed complex network.

Finally, the weighted in-degree  $ke_{v_i}$  is defined as the sum of the weights of the in-degree edges in  $v_i$ ,

$$ke_{v_i} = \sum_{v_j \in V} \begin{cases} w(e_{v_j, v_i}), & e_{v_j, v_i} \in E \\ 0, & \text{otherwise.} \end{cases} \quad (7)$$

To build a matrix of input vector for the RNN, we adopted a strategy of analysis of the evolution of the complex network for different values of the modeling parameter  $r$ . In this way, the input feature vector and the corresponding label of a vertex  $v_i$  are built according to the following procedure: the gray-scale intensity of the pixel is considered as an output label  $d_{v_i} = I(i)$  and the values of out-degree of the vertex for different values of the modeling parameter  $r$  are attributes of the input feature vector  $\vec{x}_{v_i} = [k_{v_i}^1, k_{v_i}^2, \dots, k_{v_i}^R]$ , where  $R$  is the maximum values of the modeling parameter. A matrix of input feature vectors  $X_{(k)}$  and a matrix of output labels  $D$  are then built for all the vertices of the complex network. Thus, it is possible to analyze the evolution of the topology of vertices that represent pixels that have a determined gray-scale intensity. Figure 2(a) shows an example of how to build these matrices  $X$  and  $D$ . In addition to building the matrix of input feature vectors  $X_{(k)}$  for the out-degree, we also built matrices of input vectors for the weighted out-degree  $X_{(ks)}$  and for the weighted in-degree  $X_{(ke)}$ .

The next step is to define the weights of the matrix  $W$  of the hidden layer of the RNN. In general, these weights are determined randomly in each training stage. Nevertheless, because we want our method to provide the same signature for the same texture image, it is necessary to use the same values in the matrix  $W$ . Thus, we adopted the strategy proposed in [20] and used the Linear Congruent Generator (LCG) [38, 53] in order to obtain pseudo-random uniform values for the matrix  $W$ , according to the following equation

$$V(n+1) = (a * V(n) + b) \bmod c, \quad (8)$$

where  $V$  is a random numeric sequence and  $a$ ,  $b$  and  $c$  are parameters. The sequence  $V$  has length  $E = Q * (p + 1)$ , its first value is  $V(1) = E + 1$ , and the values of the parameters are  $a = E + 2$ ,  $b = E + 3$  and  $c = E^2$  (values adopted in [20]). Hence, the matrix  $W$  is composed of the vector  $V$  divided into  $Q$  segments of length  $p + 1$ . Finally, all values of matrix  $W$  and each line of the matrix  $X$  are normalized using z-score (zero mean and unit variance).

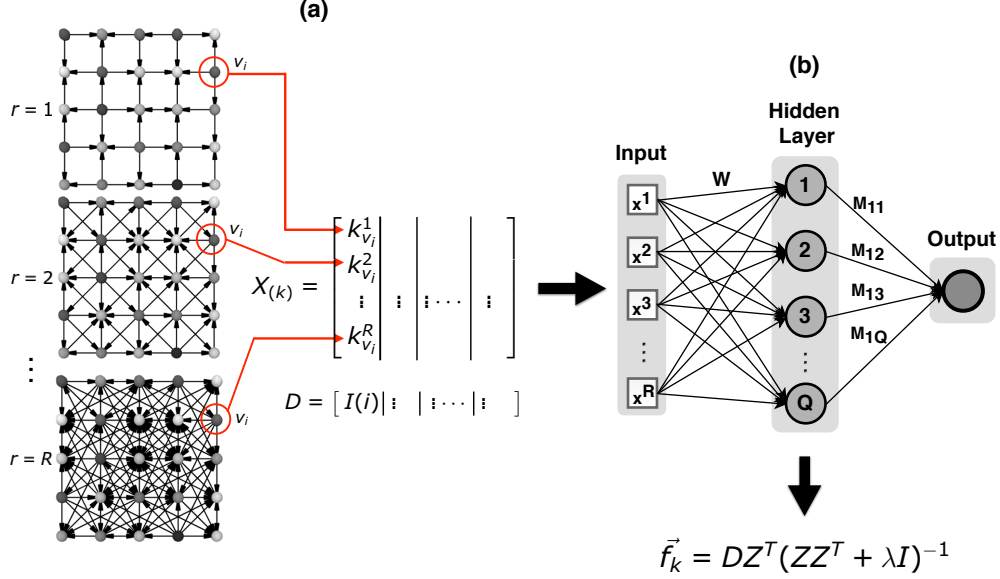


Figure 2: Building of an input feature vector and corresponding output label for the out-degree  $k_{v_i}$  using different values of  $r$  to model the complex networks.

The proposed texture signature is built based on the matrix  $M$ , which becomes a vector  $\vec{f} = DZ^T(ZZ^T + \lambda I)^{-1}$ , where  $\lambda = 10^{-3}$  (Figure 2(b)). Notice that  $\vec{f}$  has length  $Q + 1$  due to the bias weight. Thus, the first step is to concatenate the vectors  $\vec{f}$  obtained from RNNs trained with the three matrices of input data  $X_{(k)}$ ,  $X_{(k_s)}$ ,  $X_{(k_e)}$ , according to

$$\vec{\Upsilon}(Q)_R = [\vec{f}_k, \vec{f}_{k_s}, \vec{f}_{k_e}], \quad (9)$$

where  $Q$  is the number of neurons of the hidden layer and  $R$  is the maximum radius for building the complex network.

The vector  $\vec{\Upsilon}(Q)_R$  is built using a single value of  $Q$  and  $R$ . These two parameters influence the weights of the neural network and, therefore, provide different characteristics for different values. Thus, initially we propose a vector  $\vec{\Theta}(R)_{(Q_1, Q_2, \dots, Q_m)}$  that concatenates the vectors  $\vec{\Upsilon}(Q)_R$  for different values of  $Q$ ,

$$\vec{\Theta}(R)_{Q_1, Q_2, \dots, Q_m} = [\vec{\Upsilon}(Q_1)_R, \vec{\Upsilon}(Q_2)_R, \dots, \vec{\Upsilon}(Q_m)_R]. \quad (10)$$

Finally, we propose a feature vector  $\vec{\Psi}(R_1, R_2)_{Q_1, Q_2, \dots, Q_m}$  that concatenates the vector  $\vec{\Theta}(R)_{Q_1, Q_2, \dots, Q_m}$  for two values of  $R$ ,

$$\vec{\Psi}(R_1, R_2)_{Q_1, Q_2, \dots, Q_m} = [\vec{\Theta}(R_1)_{Q_1, Q_2, \dots, Q_m}, \vec{\Theta}(R_2)_{Q_1, Q_2, \dots, Q_m}]. \quad (11)$$

## 4 Experiments

In order to validate our proposed method and compare it to other texture analysis methods, the signatures were classified using linear discriminant analysis [24]. This classifier was adopted due to its simplicity, which emphasizes the characteristics obtained by the methods. The leave-one-out cross-validation scheme was used. In this validation strategy, one sample is used for testing the model and the remainder for training it. This process is repeated  $N$  times ( $N$  is the number of samples), each time with a different sample for testing. The performance measure is the average accuracy of the  $N$  runnings.

The gray-scale texture databases used as benchmark to evaluate our proposed method were:

- Brodatz [11]: just as in [5], 1776 texture images of  $128 \times 128$  pixel size from this database divided into 111 classes were used in this work.

- Outex [46]: just as in [5], the original 68 images  $746 \times 538$  from TC\_Outex\_00013 were divided into 20 sub-images  $128 \times 128$  pixel size without overlapping. Thus, the database used in this work has 1360 textures.
- USPTex [4]: this database has 2292 samples divided into 191 classes, 12 images per class, and each image has  $128 \times 128$  pixel size.
- Vistex: the database *Vision Texture* is provided by the Vision and Modeling Group - MIT Media Lab [55]. Just as in [5], the original 54 images  $512 \times 512$  were split into 16 sub-images  $128 \times 128$  pixel size without overlapping. Thus, the database used in this work has 864 images.

The proposed method is applied to the aforementioned databases and the accuracy is compared to other methods of the literature. They are: Grey-Level Co-occurrence Matrix (GLCM) [30, 31], Gray Level Difference Matrix (GLDM) [36, 63], Fourier [1], Gabor Filters [33, 42], Fractal [3], Fractal Fourier [22], Local Binary Patterns (LBP) [47], Local Binary Patterns Variance (LBPV) [29], Complete Local Binary Pattern (CLBP) [28], Local Phase Quantization (LPQ) [48], Local Configuration Pattern (LCP) [27], Local Frequency Descriptor (LFD) [40], Binarized Statistical Image Features (BSIF) [35], Local Oriented Statistics Information Booster (LOSIB) [25], Adaptive Hybrid Pattern (AHP) [67], Complex Network Texture Descriptors (CNTD) [5] and ELM signature [20].

## 5 Results and Discussion

### 5.1 Parameter Evaluation

Figure 5.1 shows the accuracies achieved on the four databases with the feature vector  $\vec{\Upsilon}(Q)_R$  using  $R = 4$ . In this experiment, we used different values of  $Q \in \{04, 09, 14, 19, 29, 39\}$ , which were selected because they produce a number of features that is multiple of five for each feature vector considered. As can be seen in the figure, the success rates increase as we increase the value of  $Q$ . This increase is followed by an increase in the number of features used. The best accuracies are obtained using  $Q = 14$  on the Vistex database and  $Q = 19$  on the other databases. These values of  $Q$  produce feature vectors of size 45 ( $Q = 14$ ) and 60 ( $Q = 19$ ). Furthermore, the success rate stabilizes when we use values of  $Q$  larger than  $Q = 14$  on the Vistex database and values larger than  $Q = 19$  on the other databases.

Table 1 shows the accuracies obtained on the four databases using the feature vector  $\vec{\Theta}(R)_{Q_1, Q_2, \dots, Q_m}$  with  $R = 4$ . The results show that as the values of  $Q$  and its combinations increase (i.e. the number of features increases), the success rates increase as well. However, very large feature vectors do not assure the highest performance, once the success rates tend to stabilize at a determined value. For instance, if we compare the vector  $\vec{\Theta}(04)_{19, 29, 39}$ , which has 270 features, with the vector  $\vec{\Theta}(04)_{04, 09, 14}$ , which has 90 attributes, the former has a lower performance in all the databases. This suggests that the proposed signature reaches its limit in terms of discrimination. Thus, we considered the vectors  $\vec{\Theta}(04)_{04, 09, 14}$  and  $\vec{\Theta}(04)_{04, 14, 19}$ , since they presented a good trade-off between high accuracy and a small number of features.

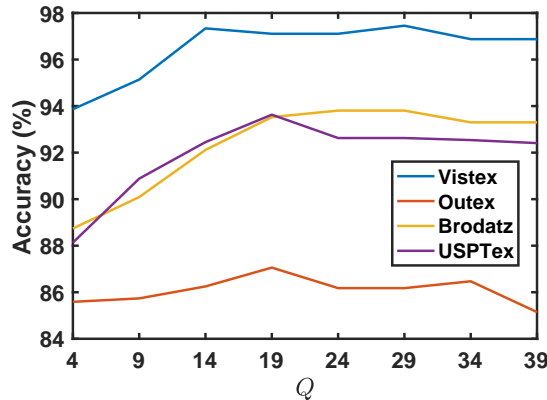


Figure 3: Accuracies of the feature vector  $\vec{\Upsilon}(Q)_R$  using different values of  $Q$  on the four databases.

We also evaluated the feature vector  $\vec{\Theta}(R)_{Q_1, Q_2, \dots, Q_m}$  for different values of  $R$ . Figure 4 shows the accuracies yielded considering the combinations  $Q = \{04, 09, 14\}$  and  $Q = \{04, 14, 19\}$ . The value of maximum radius  $R$  is associated to the zone of connection between the pixels (i.e., vertices). Thus, lower values of  $R$  represent the closest pixels and,

Table 1: Accuracies of the feature vector  $\vec{\Theta}(R)_{Q_1, Q_2, \dots, Q_m}$  using different values of  $Q$  and their combinations for the maximum radius  $R = 4$ .

$\{Q_1, Q_2, \dots, Q_m\}$	No of features	Outex	USPTex	Brodatz	Vistex
{04, 09}	45	88.60	94.07	93.02	97.22
{04, 14}	60	88.82	94.98	93.86	98.50
{04, 19}	75	88.97	95.46	94.88	97.92
{04, 29}	105	88.38	94.76	94.48	97.80
{04, 39}	135	87.57	95.42	95.27	98.15
{09, 14}	75	88.09	94.72	93.52	97.92
{09, 19}	90	88.60	94.42	94.26	98.15
{09, 29}	120	87.50	94.24	94.14	97.80
{09, 39}	150	86.76	94.81	94.88	97.80
{14, 19}	105	89.04	94.94	94.54	98.26
{14, 29}	135	88.09	94.90	94.48	97.92
{14, 39}	165	87.65	95.29	95.33	98.15
{19, 29}	150	87.50	94.59	94.76	97.45
{19, 39}	180	87.28	95.03	95.27	98.03
{29, 39}	210	85.88	94.37	95.05	97.92
<b>{04, 09, 14}</b>	<b>90</b>	<b>89.34</b>	<b>95.46</b>	<b>95.05</b>	<b>98.61</b>
{04, 09, 19}	105	89.71	95.55	95.16	98.26
{04, 09, 29}	135	88.68	95.51	94.88	97.80
{04, 09, 39}	165	87.94	95.90	95.72	97.80
<b>{04, 14, 19}</b>	<b>120</b>	<b>89.41</b>	<b>95.94</b>	<b>95.21</b>	<b>98.38</b>
{04, 14, 29}	150	88.68	95.59	95.05	98.26
{04, 14, 39}	180	88.53	95.90	95.89	98.84
{04, 19, 29}	165	89.12	95.94	95.27	98.03
{04, 19, 39}	195	88.68	95.90	95.61	98.38
{04, 29, 39}	225	87.94	95.03	95.72	98.38
{09, 14, 19}	135	89.56	95.24	94.99	98.50
{09, 14, 29}	165	88.75	95.42	95.10	98.15
{09, 14, 39}	195	88.01	95.68	95.61	98.73
{09, 19, 29}	180	88.75	95.24	94.93	98.26
{09, 19, 39}	210	87.94	95.38	95.05	97.92
{09, 29, 39}	240	88.01	94.59	94.99	97.92
{14, 19, 29}	195	88.75	95.33	95.05	98.50
{14, 19, 39}	225	88.38	95.72	95.44	98.61
{14, 29, 39}	255	88.09	95.03	95.50	98.50
{19, 29, 39}	270	88.01	94.63	95.50	97.92

as  $R$  increases, the reach of connection increases as well. The results show that the lowest values of  $R$  provide better accuracies when compared to the highest values. This demonstrates that local patterns are more important than global patterns to discriminate the textures.

Furthermore, we analyzed the combination of vectors  $\vec{\Theta}(R)_{Q_1, Q_2, \dots, Q_m}$  (showed in Table 1) with different values of maximum radius  $R$ , resulting in the vector  $\vec{\Psi}(R_1, R_2)_{Q_1, Q_2, \dots, Q_m}$ . To compute this vector, we used the combinations of  $Q$  that provided the best results in Table 1:  $Q = \{4, 9, 14\}$  and  $Q = \{4, 14, 19\}$ . In this experiment, we computed the vector  $\vec{\Psi}(R_1, R_2)_{Q_1, Q_2, \dots, Q_m}$  for two values of  $R$  (i.e. up to two combinations of  $\vec{\Theta}(R)_{Q_1, Q_2, \dots, Q_m}$ ) due to the large number of features generated.

Table 2 shows the results of the vectors  $\vec{\Psi}(R_1, R_2)_{Q_1, Q_2, \dots, Q_m}$  using the combination  $Q = \{04, 09, 14\}$ . The highest accuracy was provided by the vector  $\vec{\Psi}(04, 06)_{04, 09, 14}$ . The results of the vectors  $\vec{\Psi}(R_1, R_2)_{Q_1, Q_2, \dots, Q_m}$  built with the combination  $Q = \{04, 14, 19\}$  are shown in Table 3. In this experiment, the best results were obtained by using the vector  $\vec{\Psi}(04, 10)_{04, 14, 19}$ . Tables 2 and 3 also show that by combining the vector  $\vec{\Theta}(R)_{Q_1, Q_2, \dots, Q_m}$  with different values of  $R$ , the accuracy increases approximately 1% on the databases. However, in the two cases, the combinations of high values of  $R$  provide inferior results. Even though the best results of the two Tables ( $\vec{\Psi}(04, 06)_{04, 09, 14}$  and  $\vec{\Psi}(04, 10)_{04, 14, 19}$ ) are similar, notice that the vector  $\vec{\Psi}(04, 10)_{04, 14, 19}$  has a number of features larger than the vector  $\vec{\Psi}(04, 06)_{04, 09, 14}$ .

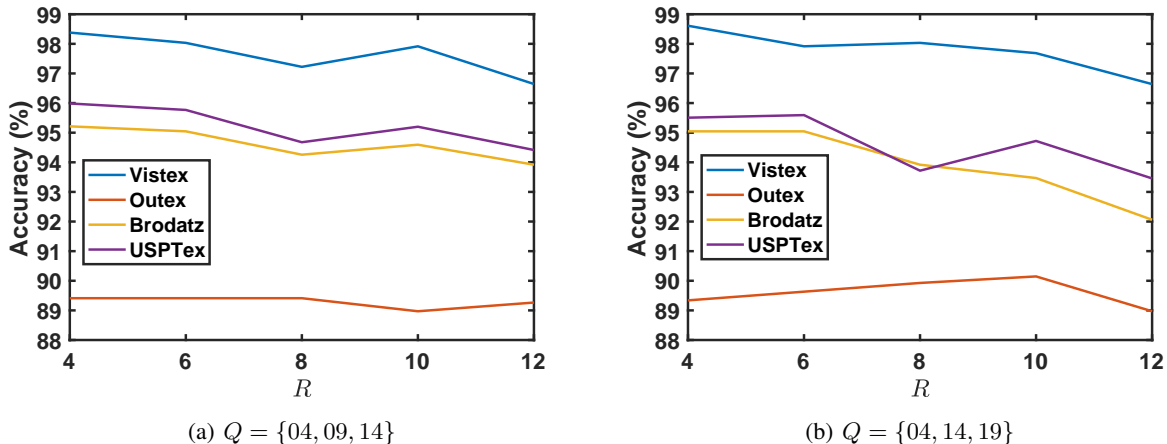


Figure 4: Accuracies using the feature vector  $\vec{\Theta}(R)_{Q_1, Q_2, \dots, Q_m}$  for the two better set of  $Q$  with different values of maximum radius  $R$ .

Table 2: Accuracies using different sets of radii  $R$  and  $Q = \{04, 09, 14\}$ .

$\{R_1, R_2\}$	No of features	Outex	USPTex	Brodatz	Vistex
<b><math>\{04, 06\}</math></b>	<b>180</b>	<b>91.54</b>	<b>96.64</b>	<b>96.11</b>	<b>98.73</b>
$\{04, 08\}$	180	91.47	96.25	95.88	98.26
$\{04, 10\}$	180	91.47	96.55	95.83	98.84
$\{04, 12\}$	180	91.69	96.25	95.72	98.26
$\{06, 08\}$	180	91.54	96.47	95.77	98.61
$\{06, 10\}$	180	90.74	96.25	95.83	98.50
$\{06, 12\}$	180	90.44	96.38	95.83	98.38
$\{08, 10\}$	180	90.58	96.03	95.15	98.49
$\{08, 12\}$	180	90.29	95.72	95.21	98.14
$\{10, 12\}$	180	90.59	95.46	94.93	98.38

Table 3: Accuracies using different sets of radii  $R$  and  $Q = \{4, 14, 19\}$ .

$\{R_1, R_2\}$	No of features	Outex	USPTex	Brodatz	Vistex
$\{04, 06\}$	240	90.07	96.73	95.83	99.19
$\{04, 08\}$	240	91.17	96.68	96.05	98.95
<b><math>\{04, 10\}</math></b>	<b>240</b>	<b>91.32</b>	<b>96.95</b>	<b>96.06</b>	<b>99.19</b>
$\{04, 12\}$	240	91.76	96.64	96.11	98.61
$\{06, 08\}$	240	90.14	96.29	96.39	98.61
$\{06, 10\}$	240	89.63	96.60	95.95	98.50
$\{06, 12\}$	240	90.29	96.55	96.06	98.26
$\{08, 10\}$	240	90.00	95.94	95.72	98.37
$\{08, 12\}$	240	91.32	95.94	95.77	98.03
$\{10, 12\}$	240	90.51	96.03	95.05	98.03

## 5.2 Comparison with other methods

To evaluate the results obtained by our proposed method, we performed comparisons with methods present in the literature. The experimental setup used was the same for all the methods (LDA with leave-one-out), except for CLBP, which used the classifier 1-Nearest Neighborhood (1-NN) with distance chi-square, according to the original paper. For our method, we adopted the two texture signatures that obtained the best results in the previous analysis:  $\vec{\Psi}(04, 06)_{04, 09, 14}$  and  $\vec{\Psi}(04, 10)_{04, 14, 19}$ .

Table 4 presents the results obtained by all the methods in the four image databases evaluated. The results show that our proposed method obtained the best results when compared to the other methods using both signatures. Also, it

Table 4: Comparison of accuracies of different texture analysis methods in four texture databases. A subset of the compared results is present in [20]

Methods	No of features	Outex	USPTex	Brodatz	Vistex
GLCM [30]	24	80.73	83.64	90.43	92.24
GLDM [63]	60	86.76	92.06	94.43	97.11
Gabor Filters [42]	48	81.91	89.22	89.86	93.29
Fourier [63]	63	81.91	67.50	75.90	79.51
Fractal [3]	69	80.51	78.27	87.16	91.67
Fractal Fourier [22]	68	68.38	59.47	71.96	79.75
LBP [47]	256	81.10	85.43	93.64	97.92
LBPV [29]	555	75.66	54.97	86.26	88.65
CLBP [28]	648	85.80	91.14	95.32	98.03
AHP [67]	120	88.31	94.85	94.88	98.38
BSIF [35]	256	77.43	77.66	91.44	88.66
LCP [27]	81	86.25	91.14	93.47	94.44
LFD [40]	276	82.57	83.55	90.99	94.68
LPQ [48]	256	79.41	85.12	92.51	92.48
ELM Signature [20]	180	89.71	95.11	95.27	98.15
CNTD [5]	108	86.76	91.71	95.27	98.03
$\vec{\Theta}(04)_{04,09,14}$	90	89.34	95.46	95.05	98.61
$\vec{\Psi}(04, 06)_{04,09,14}$	180	<b>91.54</b>	96.64	<b>96.11</b>	98.73
$\vec{\Psi}(04, 10)_{04,14,19}$	240	91.32	<b>96.95</b>	96.06	<b>99.19</b>

is important to stress that our method reached higher accuracies than the ELM signature and CNTD method (which is also based on complex networks). This suggests that our method obtained superior performance because it has simultaneously the main characteristics of both compared methods. In other words, the ELM signature uses only pixel intensities to train the neural network, without any valuable information from complex network modeling, and the CNTD method models images as complex networks and computes only traditional measures, without using a neural network to extract the deep characteristics from these complex networks.

Even though our proposed method has signatures with a larger number of descriptors when compared to some methods of the literature, it is important to emphasize that, if we consider only the vector  $\vec{\Theta}(R)_{Q_1, Q_2, \dots, Q_m}$ , the results are still competitive. For instance, the vector  $\vec{\Theta}(04)_{4,9,14}$ , which has only 90 features, provides superior performance on the Vistex and USPTex databases. In the remainder databases, the results are very close to the highest accuracies (only 0.37% smaller than the result of ELM signature on the Outex database and 0.27% smaller than the accuracy of the CLBP on the Brodatz database)

## 6 Conclusion

This paper presented an innovative approach of texture feature extraction based on the fusion of complex network and randomized neural network. In the proposed method, a new approach to model the image as a CN that uses only a parameter is presented. We also proposed a new way of characterizing the CN based on the idea of using the output weights of a randomized neural network trained with topological properties of the CN. The obtained classification results on four databases outperformed other texture literature methods. Also, the proposed approach has an excellent trade-off between performance and size of the feature vectors. This demonstrates that the proposed approach is highly discriminative using the three feature vectors considered. In this way, this paper shows that the fusion of complex network and randomized neural network is a research field with great potential as a feasible texture analysis methodology.

## Acknowledgments

Lucas Correia Ribas gratefully acknowledges the financial support grant #2016/23763-8, São Paulo Research Foundation (FAPESP). Jarbas Joaci de Mesquita Sá Junior thanks CNPq (National Council for Scientific and Technological Development, Brazil) (Grant: 302183/2017-5) for the financial support of this work. Leonardo Felipe dos Santos Scabini acknowledges support from CNPq (Grant #134558/2016-2). Odemir M. Bruno thanks the financial support of CNPq (Grant # 307797/2014-7) and FAPESP (Grant #s 14/08026-1 and 16/18809-9).

## References

- [1] AZENCOTT, R., WANG, J.-P., AND YOUNES, L. Texture classification using windowed Fourier filters. *IEEE Transactions on Pattern Analysis and Machine Intelligence* 19, 2 (1997), 148–153.
- [2] BACKES, A. R., AND BRUNO, O. M. A new approach to estimate fractal dimension of texture images. In *International Conference on Image and Signal Processing* (2008), Springer, pp. 136–143.
- [3] BACKES, A. R., CASANOVA, D., AND BRUNO, O. M. Plant leaf identification based on volumetric fractal dimension. *International Journal of Pattern Recognition and Artificial Intelligence* 23, 06 (2009), 1145–1160.
- [4] BACKES, A. R., CASANOVA, D., AND BRUNO, O. M. Color texture analysis based on fractal descriptors. *Pattern Recognition* 45, 5 (2012), 1984–1992.
- [5] BACKES, A. R., CASANOVA, D., AND BRUNO, O. M. Texture analysis and classification: A complex network-based approach. *Information Sciences* 219 (2013), 168–180.
- [6] BARABÁSI, A. L. *Network science*. Cambridge university press, 2016.
- [7] BARABÁSI, A.-L., AND ALBERT, R. Emergence of scaling in random networks. *science* 286, 5439 (1999), 509–512.
- [8] BHARATI, M. H., LIU, J., AND MACGREGOR, J. F. Image texture analysis: methods and comparisons. *Chemometrics and Intelligent Laboratory Systems* 72, 1 (2004), 57 – 71.
- [9] BOCCALETTI, S., LATORA, V., MORENO, Y., CHAVEZ, M., AND HWANG, D.-U. Complex networks: Structure and dynamics. *Physics reports* 424, 4 (2006), 175–308.
- [10] BRAHNMAM, S., JAIN, L. C., NANNI, L., LUMINI, A., ET AL. *Local binary patterns: new variants and applications*. Springer, 2016.
- [11] BRODATZ, P. *Textures: A photographic album for artists and designers*. Dover Publications, New York, 1966.
- [12] BRUNO, O. M., DE OLIVEIRA PLOTZE, R., FALVO, M., AND DE CASTRO, M. Fractal dimension applied to plant identification. *INFORMATION SCIENCES* 178, 12 (2008), 2722–2733.
- [13] CALVETTI, D., MORIGI, S., REICHEL, L., AND SGALLARI, F. Tikhonov regularization and the L-curve for large discrete ill-posed problems. *Journal of Computational and Applied Mathematics* 123, 1 (2000), 423 – 446.
- [14] CHICKLORE, S., GOH, V., SIDDIQUE, M., ROY, A., MARSDEN, P. K., AND COOK, G. J. Quantifying tumour heterogeneity in 18f-fdg pet/ct imaging by texture analysis. *European journal of nuclear medicine and molecular imaging* 40, 1 (2013), 133–140.
- [15] COSTA, L. D. F., RODRIGUES, F. A., TRAVIESO, G., AND VILLAS BOAS, P. R. Characterization of complex networks: A survey of measurements. *Advances in Physics* 56, 1 (2007), 167–242.
- [16] COVER, T. M. Geometrical and statistical properties of systems of linear inequalities with applications in pattern recognition. *IEEE Transactions on Electronic Computers EC-14*, 3 (1965), 326–334.
- [17] CSURKA, G., DANCE, C., FAN, L., WILLAMOWSKI, J., AND BRAY, C. Visual categorization with bags of keypoints. In *ECCV International Workshop on Statistical Learning in Computer Vision* (2004), pp. 1–22.
- [18] DA FONTOURA COSTA, L., JR., O. N. O., TRAVIESO, G., RODRIGUES, F. A., BOAS, P. R. V., ANTIQUEIRA, L., VIANA, M. P., AND ROCHA, L. E. C. Analyzing and modeling real-world phenomena with complex networks: a survey of applications. *Advances in Physics* 60, 3 (2011), 329–412.
- [19] DA SILVA, N. R., VAN DER WEEËN, P., DE BAETS, B., AND BRUNO, O. M. Improved texture image classification through the use of a corrosion-inspired cellular automaton. *Neurocomputing* 149 (2015), 1560–1572.
- [20] DE MESQUITA SÁ JUNIOR, J. J., AND BACKES, A. R. Elm based signature for texture classification. *Pattern Recognition* 51 (2016), 395 – 401.
- [21] DE VES, E., ACEVEDO, D., RUEDIN, A., AND BENAVENT, X. A statistical model for magnitudes and angles of wavelet frame coefficients and its application to texture retrieval. *Pattern Recognition* 47, 9 (2014), 2925 – 2939.
- [22] FLORINDO, J. B., AND BRUNO, O. M. Fractal descriptors based on Fourier spectrum applied to texture analysis. *Physica A: statistical Mechanics and its Applications* 391, 20 (2012), 4909–4922.
- [23] FLORINDO, J. B., CASANOVA, D., AND BRUNO, O. M. Fractal measures of complex networks applied to texture analysis. In *Journal of Physics: Conference Series* (2013), vol. 410, IOP Publishing, p. 012091.
- [24] FUKUNAGA, K. *Introduction to Statistical Pattern Recognition*, 2nd ed. Academic Press, 1990.

- [25] GARCÍA-OLALLA, O., ALEGRE, E., FERNÁNDEZ-ROBLES, L., AND GONZÁLEZ-CASTRO, V. Local oriented statistics information booster (losib) for texture classification. In *Pattern Recognition (ICPR), 2014 22nd International Conference on* (2014), IEEE, pp. 1114–1119.
- [26] GONÇALVES, W. N., DA SILVA, N. R., DA FONTOURA COSTA, L., AND BRUNO, O. M. Texture recognition based on diffusion in networks. *Information Sciences* 364 (2016), 51–71.
- [27] GUO, Y., ZHAO, G., AND PIETIKÄINEN, M. Texture classification using a linear configuration model based descriptor. In *BMVC* (2011), Citeseer, pp. 1–10.
- [28] GUO, Z., ZHANG, L., AND ZHANG, D. A completed modeling of local binary pattern operator for texture classification. *IEEE Transactions on Image Processing* 19, 6 (2010), 1657–1663.
- [29] GUO, Z., ZHANG, L., AND ZHANG, D. Rotation invariant texture classification using lbp variance (lbpv) with global matching. *Pattern recognition* 43, 3 (2010), 706–719.
- [30] HARALICK, R. M. Statistical and structural approaches to texture. *Proceedings of the IEEE* 67, 5 (1979), 786–804.
- [31] HARALICK, R. M., SHANMUGAM, K., AND DINSTEN, I. H. Textural features for image classification. *IEEE Transactions on systems, man, and cybernetics*, 6 (1973), 610–621.
- [32] HUANG, G.-B., ZHU, Q.-Y., AND SIEW, C.-K. Extreme learning machine: theory and applications. *Neurocomputing* 70, 1 (2006), 489–501.
- [33] IDRISSE, M., AND ACHEROY, M. Texture classification using gabor filters. *Pattern Recognition Letters* 23, 9 (2002), 1095–1102.
- [34] JAIN, A. K., AND FARROKHNI, F. Unsupervised texture segmentation using Gabor filters. In *Systems, Man and Cybernetics, 1990. Conference Proceedings., IEEE International Conference on* (1990), IEEE, pp. 14–19.
- [35] KANNALA, J., AND RAHTU, E. Bsif: Binarized statistical image features. In *Pattern Recognition (ICPR), 2012 21st International Conference on* (2012), IEEE, pp. 1363–1366.
- [36] KIM, J. K., AND PARK, H. W. Statistical textural features for detection of microcalcifications in digitized mammograms. *IEEE transactions on medical imaging* 18, 3 (1999), 231–238.
- [37] LAM, W.-K., AND LI, C.-K. Rotated texture classification by improved iterative morphological decomposition. *IEE Proceedings-Vision, Image and Signal Processing* 144, 3 (1997), 171–179.
- [38] LEHMER, D. H. Mathematical methods in large scale computing units. *Annals Comp. Laboratory Harvard University* 26 (1951), 141–146.
- [39] LIU, L., CHEN, J., FIEGUTH, P., ZHAO, G., CHELLAPPA, R., AND PIETIKAINEN, M. A survey of recent advances in texture representation. *arXiv preprint arXiv:1801.10324* (2018).
- [40] MAANI, R., KALRA, S., AND YANG, Y.-H. Noise robust rotation invariant features for texture classification. *Pattern Recognition* 46, 8 (2013), 2103–2116.
- [41] MALAMAS, E. N., PETRAKIS, E. G., ZERVAKIS, M., PETIT, L., AND LEGAT, J.-D. A survey on industrial vision systems, applications and tools. *Image and vision computing* 21, 2 (2003), 171–188.
- [42] MANJUNATH, B. S., AND MA, W.-Y. Texture features for browsing and retrieval of image data. *IEEE Transactions on pattern analysis and machine intelligence* 18, 8 (1996), 837–842.
- [43] MIRANDA, G. H. B., MACHICAO, J., AND BRUNO, O. M. Exploring spatio-temporal dynamics of cellular automata for pattern recognition in networks. *Scientific Reports* 6 (Nov 2016), 37329.
- [44] MOORE, E. H. On the reciprocal of the general algebraic matrix. *Bulletin of the American Mathematical Society* 26 (1920), 394–395.
- [45] NANNI, L., LUMINI, A., AND BRAHNAM, S. Survey on LBP based texture descriptors for image classification. *Expert Systems with Applications* 39, 3 (2012), 3634–3641.
- [46] OJALA, T., MÄENPÄÄ, T., PIETIKÄINEN, M., VIERTOLA, J., KYLLÖNEN, J., AND HUOVINEN, S. Outex: New framework for empirical evaluation of texture analysis algorithms. In *International Conference on Pattern Recognition* (2002), pp. 701–706.
- [47] OJALA, T., PIETIKAINEN, M., AND MAENPAA, T. Multiresolution gray-scale and rotation invariant texture classification with local binary patterns. *IEEE Transactions on pattern analysis and machine intelligence* 24, 7 (2002), 971–987.
- [48] OJANSIVU, V., AND HEIKKILÄ, J. Blur insensitive texture classification using local phase quantization. In *International conference on image and signal processing* (2008), Springer, pp. 236–243.

- [49] PALM, C. Color texture classification by integrative co-occurrence matrices. *Pattern recognition* 37, 5 (2004), 965–976.
- [50] PANJWANI, D. K., AND HEALEY, G. Markov random field models for unsupervised segmentation of textured color images. *IEEE Transactions on pattern analysis and machine intelligence* 17, 10 (1995), 939–954.
- [51] PAO, Y.-H., PARK, G.-H., AND SOBAJIC, D. J. Learning and generalization characteristics of the random vector functional-link net. *Neurocomputing* 6, 2 (1994), 163–180.
- [52] PAO, Y.-H., AND TAKEFUJI, Y. Functional-link net computing: theory, system architecture, and functionalities. *Computer* 25, 5 (1992), 76–79.
- [53] PARK, S. K., AND MILLER, K. W. Random number generators: good ones are hard to find. *Communications of the ACM* 31, 10 (1988), 1192–1201.
- [54] PENROSE, R. A generalized inverse for matrices. *Mathematical Proceedings of the Cambridge Philosophical Society* 51, 3 (1955), 406—413.
- [55] PICARD, R., GRACZYK, C., MANN, S., WACHMAN, J., PICARD, L., AND CAMPBELL, L. *Vision texture database*. Media Laboratory, MIT, Cambridge, Massachusetts, 1995.
- [56] RIBAS, L. C., GONÇALVES, D. N., ORUÊ, J. P. M., AND GONÇALVES, W. N. Fractal dimension of maximum response filters applied to texture analysis. *Pattern Recognition Letters* 65 (2015), 116–123.
- [57] SCABINI, L. F., CONDORI, R. H., GONÇALVES, W. N., AND BRUNO, O. M. Multilayer complex network descriptors for color-texture characterization. *Information Sciences* 491 (2019), 30 – 47.
- [58] SCABINI, L. F., GONÇALVES, W. N., AND CASTRO JR, A. A. Texture analysis by bag-of-visual-words of complex networks. In *Iberoamerican Congress on Pattern Recognition* (2015), Springer International Publishing, pp. 485–492.
- [59] SCHMIDT, W. F., KRAAIJVELD, M. A., AND DUIN, R. P. W. Feedforward neural networks with random weights. In *Proceedings., 11th IAPR International Conference on Pattern Recognition. Vol.II. Conference B: Pattern Recognition Methodology and Systems* (1992), pp. 1–4.
- [60] TIKHONOV, A. N. On the solution of ill-posed problems and the method of regularization. *Dokl. Akad. Nauk USSR* 151, 3 (1963), 501—504.
- [61] WATTS, D. J., AND STROGATZ, S. H. Collective dynamics of ‘small-world’ networks. *nature* 393, 6684 (1998), 440–442.
- [62] WENK, H. R. *Preferred Orientation in Deformed Metal and Rocks: An Introduction to Modern Texture Analysis*. Elsevier, 2013.
- [63] WESZKA, J. S., DYER, C. R., AND ROSENFELD, A. A comparative study of texture measures for terrain classification. *IEEE transactions on Systems, Man, and Cybernetics*, 4 (1976), 269–285.
- [64] XU, D., CHEN, X., XIE, Y., YANG, C., AND GUI, W. Complex networks-based texture extraction and classification method for mineral flotation froth images. *Minerals Engineering* 83 (2015), 105–116.
- [65] ZHANG, J., AND TAN, T. Brief review of invariant texture analysis methods. *Pattern recognition* 35, 3 (2002), 735–747.
- [66] ZHANG, J., AND TAN, T. Brief review of invariant texture analysis methods. *Pattern recognition* 35, 3 (2002), 735–747.
- [67] ZHU, Z., YOU, X., CHEN, C. P., TAO, D., OU, W., JIANG, X., AND ZOU, J. An adaptive hybrid pattern for noise-robust texture analysis. *Pattern Recognition* 48, 8 (2015), 2592–2608.
- [68] ZIMER, A. M., RIOS, E. C., MENDES, P. D. C. D., GONÇALVES, W. N., BRUNO, O. M., PEREIRA, E. C., AND MASCARO, L. H. Investigation of aisi 1040 steel corrosion in h2s solution containing chloride ions by digital image processing coupled with electrochemical techniques. *Corrosion Science* 53, 10 (2011), 3193–3201.